THE JOURNAL OF PHYSICAL CHEMISTRY C

ARTICLE

pubs.acs.org/JPCC

Periodically Modulated Electronic Properties of the Epitaxial Monolayer Graphene on Ru(0001)

Wei Feng, Shulai Lei, Qunxiang Li, and Aidi Zhao*

Hefei National Laboratory for Physical Sciences at Microscale, University of Science and Technology of China, Hefei, Anhui 230026, People's Republic of China

ABSTRACT: The local structural and electronic properties of the epitaxial monolayer graphene (MG) on Ru(0001) surface were investigated by using scanning tunneling microscopy/spectroscopy (STM/STS) and first-principles calculations. High resolution STM images and STS spectra measured in a large bias voltage range indicated both geometric and electronic corrugation of the MG. The local work function (LWF) of the MG/Ru(0001) surface was obtained to be around 3.5 eV by two separate methods based on the experimental dz/dV and $I-z$ curves respectively. We also found a considerable LWF difference (about 100 to 200 meV) between different sites within a unit cell of the moiré pattern of MG/Ru(0001). Furthermore, noticeable bias-polarity-dependence of the local barrier height (LBH) of MG on Ru(0001) surface was observed, supporting the existence of the Smoluchowski smoothing effect due to the presence of surface dipole moment in consequence of strong MG−Ru interactions. These findings indicate that MG/Ru(0001) can be used as an ideal template for periodic nanostructures with various applications.

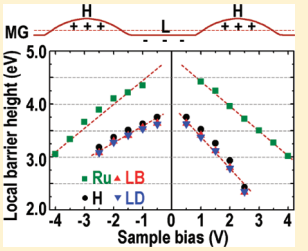

1. INTRODUCTION

Monolayer graphene (MG) is single sheet of carbon atoms arranged in a hexagonal lattice. Since the exfoliated graphene was first obtained in experiments,[1] it has attracted a lot of research interest for its intriguing physics as well as its application potential. For the extremely high mobility and the easy control of the charge carriers by applying a gate voltage, graphene has become a promising material for next-generation electronics with properties that may exceed those of conventional semiconductors. Micromechanical cleavage, however, does not appear to be a technologically relevant method for producing wafers of large size film, whereas epitaxial growth does.[2−4] Until now, graphene has been shown to epitaxially grow on some substrates, such as transition metal surfaces with thermal decomposition of hydrocarbons[5−8] and carbide.[9]

The epitaxial graphene on Ru(0001) has been studied by experiment and theory. MG with high-quality and macroscale size can continuously form on Ru(0001).[4,10] Moreover, bilayer and multilayer graphene can be prepared by controlling the growth conditions.[11] Details about the conditions of the graphene grown on Ru(0001) has been reported by Cui and his co-workers.[11,12] It is well-known that the formed MG shows the moiré pattern with a periodicity of ∼30 Å,[10,13] which is 25 × 25 graphene unit cells coinciding with 23 × 23 Ru units.[14] The periodic geometrical corrugation of MG, which has been verified,[15,16] originates from the strong chemical bonding in combination with lattice mismatch between graphene and Ru(0001).[14,17−19] The band structure of MG on Ru(0001) was analyzed with angle-resolved photoemission spectroscopy combined with density functional theory (DFT) calculations,[20] and there is linear dispersion on the humps of the corrugated layer, for these sites have a weak interaction between the atoms of C and Ru. About 0.1 e per 1 × 1 unit cell is transferred from the Ru substrate to graphene,[20,21] which means the MG on Ru(0001) is electronic doped.

Recently, MG has been investigated as a wonderful template for adsorbates[22−24] which selectively adsorb on specific sites of the moiré pattern. Site-specific adsorption on inorganic surfaces has been reported on laterally inhomogeneous surfaces before;[25−27] however, the understanding of the relevant local physical properties responsible for the site-specific substrate−adsorbate interactions remains very poor. A detailed knowledge of the local electronic properties of surfaces which includes local density of states (LDOS) and local work function (LWF), also called local surface potential, is crucial for a better understanding of a large variety of processes, ranging from electron scattering in transport phenomena to catalytic reactions.[28−30] Heretofore, numbers of studies on the MG/Ru(0001) with STM have been presented, whereas there is still a lack of systematic study on the local electronic properties as well as detailed LWF of this periodic corrugated surface.

In this paper, we present a comprehensive study on the local electronic properties and LWF of epitaxial MG on Ru(0001). The STM topographic images, dI/dV, and $I-z$ curves on the three different sites of MG surface are obtained for the investigation. The results we obtained demonstrate that there is not only a periodic geometrical corrugation on the MG surface but also a periodic distribution of the LDOS and LWF, which is further confirmed by careful DFT calculations. The STM images at low bias voltage reflect the geometrical corrugation of the MG

Received: August 27, 2011
Revised: October 31, 2011
Published: November 01, 2011

dx.doi.org/10.1021/jp2082962 | J. Phys. Chem. C 2011, 115, 24858–24864

surface; however, STM images may show inverse contrast at high bias voltage due to the emergence of electronic resonance states. Furthermore, periodic distribution of the work functions on MG was observed and the LWF differences of various sites inside a unit cell of the moiré pattern are determined. We also find a bias-polarity-dependence of the local barrier height (LBH) on the MG surface, which supports the existence of the Smoluchowski smoothing effect on the MG/Ru(0001) surface due to the presence of surface dipole moment in consequence of local MG−Ru interactions.

2. EXPERIMENT AND METHOD

All experiments were performed in an Omicron ultrahigh vacuum, low temperature STM apparatus with a base pressure of 5×10^{-11} mbar range. The Ru(0001) crystal was cleaned by cycles of Ar^+ sputtering (1000 eV) at room temperature and flash annealing to 1120 K. The graphene surface was synthesized by thermal decomposition of ethylene molecules on a Ru(0001) single crystal which was heated to 1000 K. We were able to control the graphene coverage by carefully tuning the exposing pressure and duration.[12] A coverage of 0.8 monolayer (ML) was particularly chosen for highest graphene quality for this study. All of the measurements were performed at 78 K, with an electrochemically etched tungsten tip which was subjected to Ar^+ sputtering prior to all measurements. $I-V$ curves and dI/dV curves were obtained simultaneously with the feedback loop off. dI/dV versus sample bias (V) was recorded by superimposing a small sinusoidal modulation (4 mV, 731 Hz) to the sample bias voltage, then detected the first-harmonic signal of the current through a lock-in amplifier (Stanford Research SR830). All heights (z) measured in this work were carefully calibrated with the known height of step on Au(111) surface at the same temperature. The $z-V$ spectrum was measured with the feedback loop on when the variation of the distance between tip and sample, z, was recorded as a function of the applied sample bias voltage V. The $z-V$ curves were numerically differentiated to obtain the dz/dV curves. All STM images in this work were recorded in a constant-current mode.

We used first-principles method, implemented in the Vienna Ab initio Simulation Package (VASP)[31,32] with van der Waals corrections, to study the geometric and electronic properties of the MG/Ru(0001) system. The projector-augmented wave (PAW) method in its implementation of Kresse and Joubert[33] was used to represent the electron−ion interaction. Exchange correlation interactions were described by the Perdew−Burke−Ernzerhof generalized gradient approximation (GGA).[34] The Brillouin-zone (BZ) integration was performed with single gamma k-point due to the large size of the examined supercell. The plane wave kinetic energy cutoff was set to be 400 eV. Atomic positions and lattice parameters were fully relaxed at the GGA level until the atomic forces were smaller than 0.01 eV/Å.

3. RESULTS AND DISCUSSION

STM Images of MG Surface. Figure 1A shows the constant-current STM image of 0.8 MG on Ru(0001), which was prepared by exposing heated Ru(0001) substrate (1000 K) to C_2H_4 with a pressure of 2×10^{-8} mbar for 8 min and then flash annealing to 1120 K. There are some clean Ru regions remaining on the surface, whereas other regions are covered by MG, presenting a

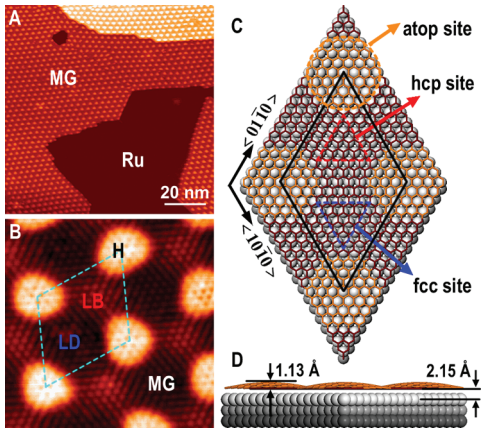

Figure 1. (A) STM image of 0.8 ML monolayer graphene (MG) on Ru(0001) (100 nm × 100 nm, acquired at $V_s = -1.0$ V and $I_t = 0.15$ nA). (B) Atomic resolved image of MG on Ru(0001) (6 nm × 6 nm, acquired at $V_s = -10$ mV and $I_t = 1.5$ nA). The unit cell of the moiré pattern on MG is marked with dash rhombus, and the three different sites are marked with H, LB, and LD, respectively. (C) The top view and (D) side view of DFT-optimized (12 × 12)C/(11 × 11) Ru(0001) structure, with the unit cell indicated as a black rhombus. The circle and triangles mark different registries of carbon atoms with respect to the Ru(0001) surface, the atop site is the honeycomb structure located on top of the Ru atom, the fcc site is the honeycomb structure located on one hollow site of the Ru lattices, and the hcp site is the honeycomb structure located on the other hollow site.

moiré pattern with a periodicity of ∼30 Å, in agreement with previous reports.[10,13] A high resolution topographic STM image of MG is shown in Figure 1B in which atomic resolution periodic patterns are clear to see. In one unit cell of the moiré pattern, there are three different sites, regardless of bias polarization in lower bias range ($|V| < \pm 2$ V): the higher sites, the brighter lower sites, and the dimmer lower sites, which is denoted with H (abbr. of higher), LB (abbr. of low brighter), and LD (abbr. of low dimmer), respectively. Unlike STM images of graphite that normally show only one of the two sublattices in the surface unit cell, the honeycomb structure of graphene is clearly resolved in H site, and the LB site shows one of the two sublattices and the LD site shows the other one.

The periodic DFT calculations were performed to mimic the experimental observed superstructure (about 3.0 nm). In our calculations, this superstructure contains a 12 × 12 lattice of repeating graphene primitive cells matching a 11 × 11 lattice of repeating Ru(0001) primitive cells along the (10$\bar{1}$0) direction, and three Ru atomic layers are used to model Ru(0001) surface. Figure 1C shows the relaxed superlattice. It is clear that there are three different symmetry sites of the carbon atom residing on the Ru lattices, marked with atop, fcc and hcp sites in Figure 1C, corresponding to the honeycomb structure residing on top of the Ru atom, on one hollow site and the other hollow site of the Ru lattices, respectively. As we know that very-low-bias (in this case $V = -10$ mV for Figure 1B) constant-current STM images will reflect real geometric contrast due to a nearly linear response of current versus applied voltage within the small energy window. These atop, fcc/hcp sites should correspond to the H, LB/LD sites in Figure 1B according to the following analysis on the geometric height differences. In the side view, as shown in Figure 1D, a hump rises from the relatively flat graphene sheet. The vertical distance between the top Ru layer and the valley sites

dx.doi.org/10.1021/jp2082962 |J. Phys. Chem. C 2011, 115, 24858–24864

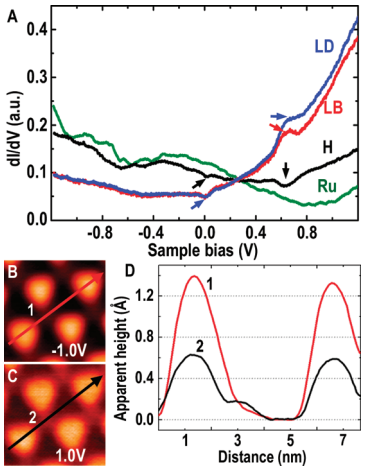

Figure 2. STM images of the MG at sample bias voltage (A) −1.0 V and (B) +1.0 V, respectively. (C) Line profile of the MG along the lines marked in (A) (red arrow) and (B) (black arrow). (D) The dI/dV curves measured on the three different sites of MG and Ru(0001) surface at V_s = 0.5 V and I_t = 0.5 nA.

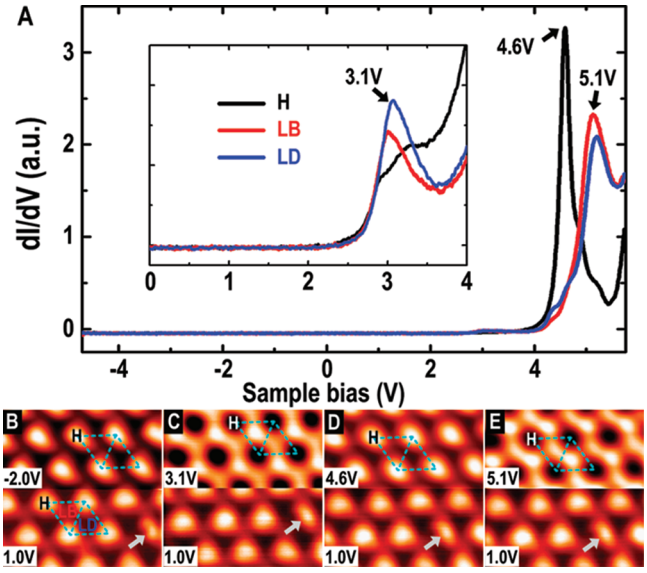

Figure 3. (A) Contrast of dI/dV curves on different sites on monolayer graphene (MG) in large sample bias range. Three black arrows show three different location of peaks at 3.1, 4.6, and 5.1 V respectively. (B−E) A set of STM images taken at the same area (a same point defect is indicated by light gray arrows) of the MG on Ru(0001) at different high sample bias voltage. The lower half of the all images were obtained at +1.0 V, and we switched the sample bias voltage in the middle of the scanning from +1.0 to −2.0, +3.1, +4.6, and +5.1 V, respectively.

of the graphene sheet is predicted to be about 2.15 Å, and the height of the hump is about 1.13 Å, which are close to the previous theoretical values.[18,19,35] The height of the hump from the above Ru layer in the H site, marked with atop site in Figure 1C, is about 3.28 Å, which is very close to the interlamellar spacing of the graphite (3.40 Å). It means that the hybrid interaction between the C atoms and the neighboring Ru atoms in the H site (atop site) is weak due to the large separation between them, and the bright honeycomb structure observed in Figure 1B is easy to be understood in the H site. Although the heights of the LB (hcp site) and LD (fcc site) sites are almost the same (about 0.02 Å in difference), as shown in Figure 1D, the atomic resolved image on the LB and LD sites displays slight difference in their STM images (Figure 1B) due to the different local chemical environments at hcp and fcc sites. In this way, we are able to identify different sites and to further verify the corresponding electronic properties of these sites of the MG on Ru(0001).

STS of the MG Surface. To study the electronic properties of the MG surface, STS with high resolution was employed. In Figure 2A, we show dI/dV curves measured on the three different sites of MG with sample bias voltage ramps from −1.2 to +1.2 V. Similar dI/dV spectra are found on LD and LB sites with slight difference, while significant different spectra are found on H sites: dI/dV spectra of H site show enhanced local density of states (LDOS) in filled states whereas LDOS of LB and LD sites are strongly enhanced in empty states. However, we did not observe an inverse contrast of STM images in this bias range, for example, STM images of a same area obtained at −1.0 and +1.0 V show similar patterns (Figure 2, panels B and C) but with changed contrast. Line profiles show that the apparent height difference between the H and LD sites varies from 1.4 to 0.6 Å for −1.0 and +1.0 V, respectively, as shown in Figure 2D. The STS spectra suggests that the LDOS of MG on Ru(0001) are periodically modulated along with the geometric corrugation, which agrees well with the previous works.[6,36,37] We also observe some fine features in the measured dI/dV curves as followings. (1) There is a resonance peak at 0.65 V for the L sites which may be associated with the π orbital of the graphene.[38] An antiresonance valley in the H site lies at 0.64 V, but its origination is unclear. (2) A dip on the Fermi energy is found for all the H, LB and LD sites, which is speculated to arise from the phonon-mediated inelastic tunnelling process as discovered in the STS of MG on oxide.[39,40] These features are intrinsic and repeatable regardless of different tips used and different areas of the surface. Detailed analysis of these fine features is beyond the discussion of the present work.

In the following, we will show the significant electronic modulation superimposed on the topographic corrugation can be further confirmed by STS measurements on MG surface in a larger bias range from −4.6 to +6.0 V. The dI/dV curves of all three sites are shown in Figure 3A, which display large variations in the empty states at higher positive sample bias voltages: Prominent resonant peaks at around +3.1 and +5.1 V were found in the dI/dV spectra of both LB and LD sites with slight difference in peak positions, whereas the dI/dV spectra of H site show sharp a resonant peak at +4.6 V and broad shoulders around 3.1 V (Figure 3A). In contrast, we did not find notable resonance at higher negative bias voltages. These resonances are so strong that significant electronic modulation on the MG can be observed directly from the STM images at sample bias voltages corresponding to the resonant peaks, as shown in Figure 3B−E. These topographic images were taken at the same area indicating with a white arrow on a same point defect. The lower halves of all the images were initially obtained at 1.0 V, and we switched the sample bias voltage in the middle of the scanning from +1.0 to −2.0, +3.1, +4.6, and +5.1 V, respectively. The upper halves of Figure 3, panels C and E, show dramatic inverse contrast comparing to their own topology. That means electron tunneling into L sites is greatly enhanced at these two bias voltages (+3.1 and +5.1 V), resulting in an inverse contrast in constant-current STM images. The attribution of these resonances will be discussed next along with the LWF results.

dx.doi.org/10.1021/jp2082962 |J. Phys. Chem. C 2011, 115, 24858–24864

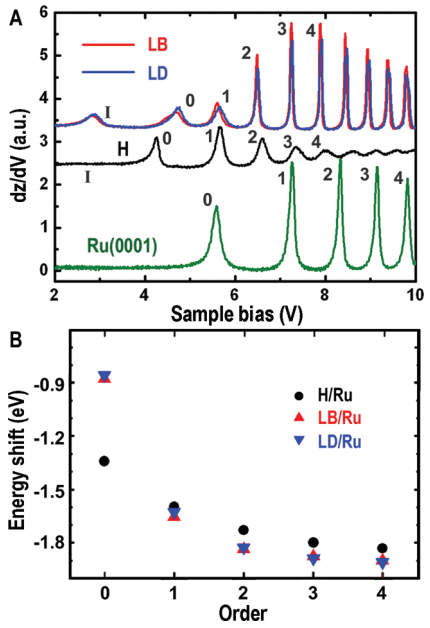

Figure 4. (A) The contrast of dz/dV−V curves obtained on MG and Ru(0001). Peak "I" is a new interfacial state, numbers (from "0" to "4") mark the order of the Gundlach oscillations. (B) Energy shift between peaks of the same order as a function of the order for curves in (A). The peaks of the Ru are used as the reference.

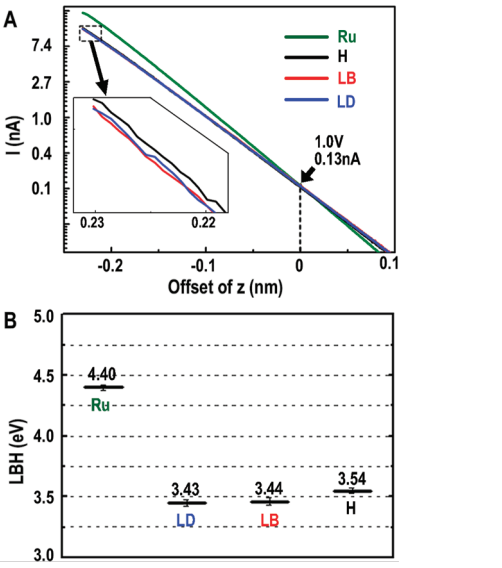

Figure 5. (A) Averaged I−z curves of different sites on MG and Ru surface, z is the distance between the tip and the sample, we set the z as reference point (z = 0 nm) when the tunnelling condition is 1.0 V and 0.13 nA. The offset of z become negative when the tip get close to the sample. Inset of (A): zoom of a segment of the I−z curves marked with dash square, there is obvious different between on the H and L sites. (B) The LBH of different sites on sample surface calculated from I−z curves in (A).

Local Work Function of the MG Surface. Two separate methods, based on the dz/dV curves in field-emission region and the estimated LBH measurements from I−z curves, were used to measure the LWF of the surface.

It is well-known that the dI/dV spectra are proportional to the LDOS of the sample only when the sample bias is much less than the work function of the sample surface. Whereas, with the applied sample bias voltage is close to or larger than the surface work function, some sharp resonances, known as the Gundlach oscillations, will appear in the tunnelling junction. The Gundlach oscillation is a phenomenon of field-emission resonance through standing-wave states in the tip−sample gap, which has been successfully employed to identify different metals[41] or to study modulations on the surface work function.[28,42,43] In a previous work,[43] it has been demonstrated that higher order Gundlach oscillations can be used to determine precisely the work function differences of thin metal films. In Figure 4A, we show dz/dV curves obtained on Ru, H, LB, and LD sites. The curves agree well with previous report.[44] But here, the curves are further used to extract the LWF difference of these different sites. According to the work by Borca et al.,[44] the first peak (at about 2.8 V) on MG surface marked with "I" in Figure 4A does not correspond to a Gundlach oscillation but originates from a new interfacial state due to the hybridization between the Ru surface state and the first image state of graphene, mostly localized on L sites. Interestingly, the peak position corresponds well to the onset of the resonance at +3.1 V in Figure 3A. It is not straightforward to correlate dI/dV spectra to dz/dV spectra because these two methods are taken in different disciplines: the former is taken in a constant height mode and the latter is taken in constant current mode. Considering a resonance in dz/dV curves means a step in the z−V curves when current is kept constant. It is not difficult to understand that at the same voltage there should be correspondingly an enhancement in current if z is fixed, i.e., in I−V measurements. As we know an enhancement of current in I−V curves is indeed corresponding to a step in dI/dV spectra, it is now clear that a resonant peak in dz/dV curve should correspond to the onset of resonance in dI/dV spectra. Peaks in Figure 4A with higher bias voltages than the interfacial state I are ascribed to Gundlach oscillations in relation to LWF. The marked numbers (from "0" to "4") for these peaks denote the order of Gundlach oscillations. In order to estimate the energy shift between different sites of MG and bare Ru surface, corresponding Gundlach peaks of Ru(0001) surface are employed as references. Figure 4B shows the energy shift of peaks with the same order as a function of the order number at different sites. For order number larger than 1, a significant energy shift was found between the bare Ru surface and MG, enlarging from ∼1.6 to ∼1.8 eV with the order number increasing from 2 to 4. The work function of Ru(0001) surface has been predicted to be about 5.4 eV.[45] Therefore, the work function of MG surface could be thus deduced to be around 3.6 eV. Differed from case of a flat film, where the energy shift of flat film remains constant as increasing order of the peaks,[43] the increasing energy shift for MG in this case is speculated to arise from the Smoluchowski smoothing effect,[46] which will be discussed later in more detail. Note that there is also an energy difference (∼0.1 eV) between the H and L sites, and the energy shifts for LB and LD sites are undistinguishable probably due to the broadening of the dz/dV peaks.

The above results do show periodically modulated LWF of MG on Ru(0001) surface. However, this method is neither straightforward nor accurate enough. It can only give LWF difference, an accurate value with known work function has to be used as reference if one need to get exact values of the LWF. A more efficient method to determine the LWF is to measure the

dx.doi.org/10.1021/jp2082962 |J. Phys. Chem. C 2011, 115, 24858–24864

LBH. Now we turn to estimate the LWF using the LBH method. The LBH measured with an STM apparatus is defined as[47,48]

$$\Phi = \frac{\hbar^2}{8m_e}\left(\frac{d}{dz}\ln I\right)^2 \cong 0.952\left(\frac{d}{dz}\ln I\right)^2$$

where I, z, m_e, $\hbar$, and Φ are tunneling current, tip−sample separation, electron mass, reduced Plank's constant $h/2\pi$, and the measured LBH. Note the measured LBH is not the LWF but the mean value of the work function of the tip Φ_T and the sample Φ_S, i. e., $\Phi = (\Phi_T + \Phi_S)/2$. The LBH can be calculated by this formula from measured $I-z$ curves. Recently, this method has been demonstrated to successfully draw the potential landscape of a single molecule−metal contact with intermolecular resolution.[49] Figure 5A shows the typical $I-z$ curves in logarithmic coordinate measured on MG and Ru at the sample bias voltage 1.0 V and current 0.13 nA. All curves show exponential decay feature with the increasing tip−sample distance. The calculated LBH on different surface sites are shown in Figure 5B with horizontal black lines. When the sample bias voltage is set to 1.0 V, the LBH on Ru(0001) surface is 4.40 ± 0.02 eV, whereas much lower LBH values are found on LD, LB, and H sites, which are 3.43 ± 0.04, 3.44 ± 0.03, and 3.54 ± 0.02 eV, respectively (the probability of bilateral confidence interval is 0.95). In our experiments, three different W tips are used to verify the repeatability of the $I-z$ curves. The deviations came mainly from the different tips used with slight varied Φ_T. Since the LBH difference of two different sites of the surface is half of the LWF difference between different surfaces $\Delta\Phi = (\Phi_{S1} - \Phi_{S2})/2$, the LWF difference between Ru and MG can be derived to be around 1.8 eV. This value coincides very well with the energy shift obtained from previous dz/dV curves.

According to the Wigner and Bardeen's work,[50] the work function of the metal can be divided into two parts: the volume contribution arising from the binding energy of the electron in the metal as a whole and the energy necessary to penetrate the double layer at the surface. If the double layer has a moment M normal to the surface which we define its sign as positive when the positive charge is on the outside and the negative charge on the inside of the surface, the work function is given by $\Phi = A - 4\pi eM$, where A, e, and M are the volume contribution mentioned before, charge of electron, and the surface moment.[46] It has been well-accepted that MG on Ru(0001) is electronically doped,[20,21] and the graphene sheet interacts more strongly with the Ru substrate at the L sites than at the H site.[6,17,19,36,51] Thus, it is expected that the charge transfer concentrate on the L sites of the moiré pattern due to the strong chemical interaction.[18,19] The charge distribution will induce a moment pointing from more negatively charged L sites to the less influenced H site. Considering the geometric corrugation of the MG, there should be a considerable component of the surface moment pointing outward in the normal axis. Now we move to the so-called Smoluchowski smoothing effect.[46] This effect was originally found as the observation of work function variations on stepped surfaces of a metal crystal, where a dipole with a component normal to the surface forms by smearing out of charge density at steps. Here we refer this effect to a general statement of work function variation induced by out-of-surface dipole formation as a consequence of geometric corrugation of the surface layer. Because of its electric dipole nature, this effect should be examined by a field-dependent behavior in local electric measurements of work function, as we will show later. According to

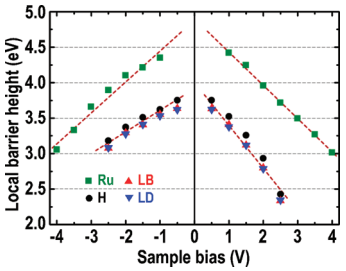

Figure 6. Variation of the LBH on different sites versus sample bias when the tunnelling current is set as a constant (0.13 nA). The bias-polarity-dependent interaction between the tip and the surface is obvious on MG surface.

the Smoluchowski's scenario,[46] the dipole moment M in this case is positive, so the work function of the corrugated MG surface should be reduced with respect to a flat MG.

In our experiment, the LBH of H site (about 3.54 eV) is about 100 meV higher than that of L sites (about 3.44 eV), which confirms the existence of a corrugated electrostatic potential surface, and also supports the existence of the Smoluchowski smoothing effect. As for the LB and LD sites, the LBH difference of the LB and LD sites (0.01 eV) is not distinguishable due to the relatively larger errors for both sites.

To further confirm the existence of the Smoluchowski smoothing effect due to the geometric corrugation of the MG surface and inhomogeneity of the electron transfer, we obtained the LBH versus the sample bias voltage of MG and Ru surfaces, as shown in Figure 6A. Because the electric dipole moment is easily affected by the electric field, there is prominent bias-polarity-dependent interaction between the tip and the surface with this smoothing effect.[52] Note that there is no Smoluchowski smoothing effect on a flat homogeneous surface; one would expect a symmetric bias-polarity behavior of the LBH at different bias voltages. This is confirmed by our data of the LBH of the bare Ru(0001) surface (square dots in Figure 6A). The LBH gradually drops with increasing of bias voltage in either polarity, which is quite reasonable because the applied bias voltage lowers the barrier height in the STM gap.[53] At the zero bias voltage limit, the LBH reaches around 4.9 eV, which is close to the mean value of the work function of Ru(0001) (5.4 eV)[45] and W(111) (4.47 eV)[54] used for the probing tip. In contrast to the symmetric bias-polarity behavior of the LBH of Ru, the slopes of the LBH for the three different sites of MG surface all show remarkable asymmetric behavior: the LBH drops more quickly with the increasing of the positive bias voltage than that of with applying negative sample bias voltage. It is easy to understand, an electric field pointing from the sample to the tip forms when we apply a positive sample bias voltage. When the bias voltage increases, the positive dipole moment M becomes larger since it is on the same direction with the applied electric field, and the LBH drops more quickly. On the contrary, the LBH drops more slowly for the dipole moment M becomes smaller as increasing the negative sample bias voltage. At the zero bias voltage limit, the LBH of the MG surface reaches around Φ = 4.0 eV. Considering the known work function of the W tip as Φ_T = 4.47 eV,[54] the averaged LWF of whole MG surface could be calculated to be around $\Phi_S = 2\Phi - \Phi_T$ = 3.53 eV. This value agrees very well with our previous result (3.6 eV) derived from the dz/dV curves. It is also close to the previous theoretical calculated work function of the MG/Ru(0001),[35] but it is slight smaller than the experimental

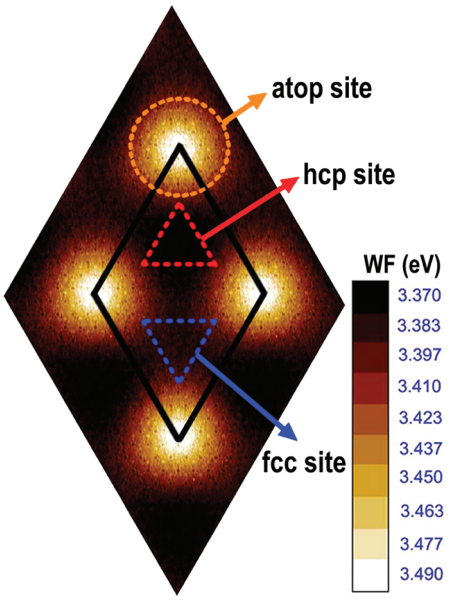

Figure 7. Calculated LWF distribution in a moiré unit cell. The three different symmetric sites marked with atop site, fcc site and hcp site are corresponding to these sites of the DFT-optimized structure in Figure 1C.

result (3.9 eV) with measured UPS.[20] For the Smoluchowski smoothing effect arises from the surface dipole moment, the work function of the MG on Ru(0001) is much smaller than that of a freestanding graphene (4.5 eV).[55] For different sample bias voltages, the LBH difference between H and L sites varies in a range of 70 to 140 meV. One would thus expect that the LWF difference between the H and L sites is in the range of 140 to 280 meV. This value compares reasonably with the LWF difference (about 100 meV, obtained from the dz/dV curves). Moreover, this result also corresponds well with the measured 240 meV electrostatic potential energy difference reported in previous work of photoemission spectroscopy.[20]

To understand these experimentally observations, we performed DFT calculations of the work function of the MG/Ru(0001). Here, Ru(0001) surface was modeled with a primitive 1 × 1 unit cell with 15 atomic slab layers, the examined MG/Ru(0001) system was illustrated in Figure 1C. The work function of the Ru (0001) was predicted to be 5.02 eV, which agrees well with the previous reported value (5.1 eV).[56] The LWF of MG/Ru(0001) surface at the H, LB, and LD sites (corresponding to the atop, fcc, and hcp sites) are 3.49, 3.39, and 3.37 eV, respectively. The simulated result indicates that the work function of the MG surface is relatively small, and the LWF differences between different sites coincide nicely with the experimental values obtained from the dz/dV and $I-z$ measurements. Figure 7 shows the spatial distribution of the work function within the supercell (the moiré pattern) of the MG/Ru(0001) system. Clearly, the work function mapping of the H, LB and LD sites is distinguishable. From the above presented experimental and theoretical results, we observe not only the geometric corrugation of MG on Ru (0001) surface, but also the variation of its electrostatic potential energy.

4. CONCLUSIONS

In summary, the geometric and electronic structures of the MG on Ru (0001) surface were studied using STM images, STS, and theoretical simulations. The inhomogeneous geometric and electronic structures of the MG/Ru(0001) were observed. The atomic-resolved topographic STM images at low bias voltage mainly reflect the geometrical corrugation, while the image contrast will inverse at high bias voltage due to the presentence of electronic resonance states. The measured STS curves depend on the location within the moiré pattern of MG on Ru(0001) surface. The LDOS at the H, LB, and LD sites are obvious different. On the basis of our experimental dz/dV and $I-z$ results, the LWF of the MG/Ru(0001) was estimated to be about 3.5 eV and the LWF difference between the H and L (LD and LB) sites is about 100 to 200 meV. The bias-polarity-dependence of the LBH of MG on the Ru(0001) surface supports the existence of the Smoluchowski smoothing effect due to the surface dipole moment, which results from the surface geometric corrugation and the inhomogeneity of the electron transfer between the MG and Ru(0001) surface. The position-depend LWF and the surface dipole ensure the MG/Ru(0001) can act as an ideal template for various applications, such as the self-assembly of molecules and clusters.

AUTHOR INFORMATION

Corresponding Author
*E-mail: adzhao@ustc.edu.cn.

ACKNOWLEDGMENT

We are grateful to Prof. J. G. Hou, Prof. B. Wang, and Prof. J. L. Yang for helpful discussions. This work was partially supported by the National Basic Research Program of China (Grant Nos. 2011CB921400 and 2010CB923300), by the National Natural Science Foundation of China (Grant Nos. 50721091, 20703041, 90921013, 11074236, 11074235, and 11034006), by the Fundamental Research Funds for the Central Universities (Grant No. WK2340000007), by the Knowledge Innovation Program of the Chinese Academy (Grant No. KJCX2-YW-W22), and by Shanghai Supercomputer Center.

REFERENCES

(1) Novoselov, K. S.; Geim, A. K.; Morozov, S. V.; Jiang, D.; Zhang, Y.; Dubonos, S. V.; Grigorieva, I. V.; Firsov, A. A. *Science* **2004**, *306*, 666–669.

(2) Li, X. S.; Cai, W. W.; An, J. H.; Kim, S.; Nah, J.; Yang, D. X.; Piner, R.; Velamakanni, A.; Jung, I.; Tutuc, E.; Banerjee, S. K.; Colombo, L.; Ruoff, R. S. *Science* **2009**, *324*, 1312–1314.

(3) Kim, K. S.; Zhao, Y.; Jang, H.; Lee, S. Y.; Kim, J. M.; Kim, K. S.; Ahn, J. H.; Kim, P.; Choi, J. Y.; Hong, B. H. *Nature* **2009**, *457*, 706–710.

(4) Sutter, E.; Albrecht, P.; Sutter, P. *Appl. Phys. Lett.* **2009**, *95*, 133109.

(5) Klusek, Z.; Kozlowski, W.; Waqar, Z.; Datta, S.; Burnell-Gray, J. S.; Makarenko, I. V.; Gall, N. R.; Rutkov, E. V.; Tontegode, A. Y.; Titkov, A. N. *Appl. Surf. Sci.* **2005**, *252*, 1221–1227.

(6) de Parga, A. L. V.; Calleja, F.; Borca, B.; Passeggi, M. C. G.; Hinarejos, J. J.; Guinea, F.; Miranda, R. *Phys. Rev. Lett.* **2008**, *100*, 056807.

(7) Kwon, S. Y.; Ciobanu, C. V.; Petrova, V.; Shenoy, V. B.; Bareno, J.; Gambin, V.; Petrov, I.; Kodambaka, S. *Nano Lett.* **2009**, *9*, 3985–3990.

(8) Wang, B.; Caffio, M.; Bromley, C.; Fruchtl, H.; Schaub, R. I. *ACS Nano* **2010**, *4*, 5773–5782.

(9) Berger, C.; Song, Z. M.; Li, X. B.; Wu, X. S.; Brown, N.; Naud, C.; Mayou, D.; Li, T. B.; Hass, J.; Marchenkov, A. N.; Conrad, E. H.; First, P. N.; de Heer, W. A. *Science* **2006**, *312*, 1191–1196.

(10) Pan, Y.; Zhang, H. G.; Shi, D. X.; Sun, J. T.; Du, S. X.; Liu, F.; Gao, H. J. *Adv. Mater.* **2009**, *21*, 2777.
(11) Cui, Y.; Fu, Q.; Bao, X. H. *Phys. Chem. Chem. Phys.* **2010**, *12*, 5053–5057.
(12) Zhang, H.; Fu, Q.; Cui, Y.; Tan, D. L.; Bao, X. H. *J. Phys. Chem. C* **2009**, *113*, 8296–8301.
(13) Marchini, S.; Gunther, S.; Wintterlin, J. *Phys. Rev. B* **2007**, *76*, 075429.
(14) Martoccia, D.; Willmott, P. R.; Brugger, T.; Bjorck, M.; Gunther, S.; Schleputz, C. M.; Cervellino, A.; Pauli, S. A.; Patterson, B. D.; Marchini, S.; Wintterlin, J.; Moritz, W.; Greber, T. *Phys. Rev. Lett.* **2008**, *101*, 126102.
(15) Martoccia, D.; Bjorck, M.; Schleputz, C. M.; Brugger, T.; Pauli, S. A.; Patterson, B. D.; Greber, T.; Willmott, P. R. *New J. Phys.* **2010**, *12*, 043028.
(16) Moritz, W.; Wang, B.; Bocquet, M. L.; Brugger, T.; Greber, T.; Wintterlin, J.; Gunther, S. *Phys. Rev. Lett.* **2010**, *104*, 136102.
(17) Preobrajenski, A. B.; Ng, M. L.; Vinogradov, A. S.; Martensson, N. *Phys. Rev. B* **2008**, *78*, 073401.
(18) Wang, B.; Bocquet, M. L.; Marchini, S.; Gunther, S.; Wintterlin, J. *Phys. Chem. Chem. Phys.* **2008**, *10*, 3530–3534.
(19) Jiang, D. E.; Du, M. H.; Dai, S. *J. Chem. Phys.* **2009**, *130*, 074705.
(20) Brugger, T.; Gunther, S.; Wang, B.; Dil, J. H.; Bocquet, M. L.; Osterwalder, J.; Wintterlin, J.; Greber, T. *Phys. Rev. B* **2009**, *79*, 045407.
(21) Kong, L. M.; Bjelkevig, C.; Gaddam, S.; Zhou, M.; Lee, Y. H.; Han, G. H.; Jeong, H. K.; Wu, N.; Zhang, Z. Z.; Xiao, J.; Dowben, P. A.; Kelber, J. A. *J. Phys. Chem. C* **2010**, *114*, 21618–21624.
(22) Mao, J. H.; Zhang, H. G.; Jiang, Y. H.; Pan, Y.; Gao, M.; Xiao, W. D.; Gao, H. J. *J. Am. Chem. Soc.* **2009**, *131*, 14136–14137.
(23) Donner, K.; Jakob, P. *J. Chem. Phys.* **2009**, *131*, 164701.
(24) Zhou, Z. H.; Gao, F.; Goodman, D. W. *Surf. Sci.* **2010**, *604*, L31–L38.
(25) Vladimirova, M.; Stengel, M.; De Vita, A.; Baldereschi, A.; Bohringer, M.; Morgenstern, K.; Berndt, R.; Schneider, W. D. *Europhys. Lett.* **2001**, *56*, 254–260.
(26) Xiao, W. D.; Ruffieux, P.; Ait-Mansour, K.; Groning, O.; Palotas, K.; Hofer, W. A.; Groning, P.; Fasel, R. *J. Phys. Chem. B* **2006**, *110*, 21394–21398.
(27) Barth, J. V. *Annu. Rev. Phys. Chem.* **2007**, *58*, 375–407.
(28) Ruffieux, P.; Aït-Mansour, K.; Bendounan, A.; Fasel, R.; Patthey, L.; Gröning, P.; Gröning, O. *Phys. Rev. Lett.* **2009**, *102*, 086807.
(29) Wandelt, K. *Appl. Surf. Sci.* **1997**, *111*, 1–10.
(30) Dil, H.; Lobo-Checa, J.; Laskowski, R.; Blaha, P.; Berner, S.; Osterwalder, J.; Greber, T. *Science* **2008**, *319*, 1824–1826.
(31) Kresse, G.; Furthmuller, J. *Phys. Rev. B* **1996**, *54*, 11169–11186.
(32) Kresse, G.; Furthmuller, J. *Comput. Mater. Sci.* **1996**, *6*, 15–50.
(33) Kresse, G.; Joubert, D. *Phys. Rev. B* **1999**, *59*, 1758–1775.
(34) Perdew, J. P.; Burke, K.; Ernzerhof, M. *Phys. Rev. Lett.* **1996**, *77*, 3865–3868.
(35) Wang, B.; Gunther, S.; Wintterlin, J.; Bocquet, M. L. *New J. Phys.* **2010**, *12*, 043041.
(36) de Parga, A. L. V.; Calleja, F.; Borca, B.; Passeggi, M. C. G.; Hinarejos, J. J.; Guinea, F.; Miranda, R. *Phys. Rev. Lett.* **2008**, *101*, 099704.
(37) Borca, B.; Barja, S.; Garnica, M.; Hinarejos, J. J.; Parga, A. L. V. d.; Miranda, R.; Guinea, F. *Semicond. Sci. Technol.* **2010**, *25*, 034001 (1−7).
(38) Byszewski, P.; Klusek, Z.; Pierzgalski, S.; Datta, S.; Kowalska, E.; Poplawska, M. *J. Electron Spectrosc. Relat. Phenom.* **2003**, *130*, 25–32.
(39) Zhang, Y. B.; Brar, V. W.; Wang, F.; Girit, C.; Yayon, Y.; Panlasigui, M.; Zettl, A.; Crommie, M. F. *Nat. Phys.* **2008**, *4*, 627–630.
(40) Brar, V. W.; Wickenburg, S.; Panlasigui, M.; Park, C. H.; Wehling, T. O.; Zhang, Y. B.; Decker, R.; Girit, C.; Balatsky, A. V.; Louie, S. G.; Zettl, A.; Crommie, M. F. *Phys. Rev. Lett.* **2010**, *104*, 036805.
(41) Jung, T.; Mo, Y. W.; Himpsel, F. J. *Phys. Rev. Lett.* **1995**, *74*, 1641–1644.
(42) Pivetta, M.; Patthey, F.; ccedil; ois; Stengel, M.; Baldereschi, A.; Schneider, W.-D. *Phys. Rev. B* **2005**, *72*, 115404.
(43) Lin, C. L.; Lu, S. M.; Su, W. B.; Shih, H. T.; Wu, B. F.; Yao, Y. D.; Chang, C. S.; Tsong, T. T. *Phys. Rev. Lett.* **2007**, *99*, 216103.
(44) Borca, B.; Barja, S.; Garnica, M.; Sanchez-Portal, D.; Silkin, V. M.; Chulkov, E. V.; Hermanns, C. F.; Hinarejos, J. J.; de Parga, A. L. V.; Arnau, A.; Echenique, P. M.; Miranda, R. *Phys. Rev. Lett.* **2010**, *105*, 036804.
(45) Himpsel, F. J.; Christmann, K.; Heimann, P.; Eastman, D. E.; Feibelman, P. J. *Surf. Sci. Lett.* **1982**, *115*, 159–164.
(46) Smoluchowski, R. *Phys. Rev.* **1941**, *60*, 661–674.
(47) Binnig, G.; Rohrer, H.; Gerber, C.; Weibel, E. *Appl. Phys. Lett.* **1982**, *40*, 178–180.
(48) Binnig, G.; Garcia, N.; Rohrer, H. *Phys. Rev. B* **1984**, *30*, 4816–4818.
(49) Vitali, L.; Levita, G.; Ohmann, R.; Comisso, A.; De Vita, A.; Kern, K. *Nat. Mater.* **2010**, *9*, 320–323.
(50) Wigner, E.; Bardeen, J. *Phys. Rev.* **1935**, *48*, 84.
(51) Altenburg, S. J.; Kr; ouml; ger, J.; Wang, B.; Bocquet, M. L.; Lorente, N.; Berndt, R. *Phys. Rev. Lett.* **2010**, *105*, 236101.
(52) Mizutani, W.; Ishida, T.; Choi, N.; Uchihashi, T.; Tokumoto, H. *Appl. Phys., A* **2001**, *72*, S181–S184.
(53) Schuster, R.; Barth, J. V.; Wintterlin, J.; Behm, R. J.; Ertl, G. *Ultramicroscopy* **1992**, *42−44*, 533–540.
(54) Michaelson, H. B. *J. Appl. Phys.* **1977**, *48*, 4729–4733.
(55) Giovannetti, G.; Khomyakov, P. A.; Brocks, G.; Karpan, V. M.; van den Brink, J.; Kelly, P. J. *Phys. Rev. Lett.* **2008**, *101*, 026803.
(56) Sun, J. T.; Du, S. X.; Xiao, W. D.; Hu, H.; Zhang, Y. Y.; Li, G.; Gao, H. J. *Chin. Phys. B* **2009**, *18*, 3008–3013.